RESEARCH ARTICLE | JUNE 14 2023

Sucrose transport inside the phloem: Bridging hydrodynamics and geometric characteristics

Mazen Nakad ; Jean-Christophe Domec ; Sanna Sevanto ; Gabriel Katul

Physics of Fluids 35, 061905 (2023)
https://doi.org/10.1063/5.0151644

Physics of Fluids ARTICLE pubs.aip.org/aip/pof

Sucrose transport inside the phloem: Bridging hydrodynamics and geometric characteristics

Cite as: Phys. Fluids **35**, 061905 (2023); doi: 10.1063/5.0151644
Submitted: 23 March 2023 · Accepted: 31 May 2023 ·
Published Online: 14 June 2023

Mazen Nakad,[1,a)] Jean-Christophe Domec,[2,3] Sanna Sevanto,[4] and Gabriel Katul[1,3]

AFFILIATIONS

[1]Department of Civil and Environmental Engineering, Duke University, Durham, North Carolina 27708, USA
[2]UMR 1391 INRA-ISPA, Bordeaux Sciences Agro, Gradignan, France
[3]Nicholas School of the Environment, Duke University, Durham, North Carolina 27708, USA
[4]Earth and Environmental Sciences Division, Los Alamos National Laboratory, Los Alamos, New Mexico 87545, USA

[a)]**Author to whom correspondence should be addressed:** mazen.nakad@gmail.com

ABSTRACT

In plants, the delivery of the products of photosynthesis is achieved through a hydraulic system labeled as phloem. This semi-permeable plant tissue consists of living cells that contract and expand in response to fluid pressure and flow velocity fluctuations. The Münch pressure flow theory, which is based on osmosis providing the necessary pressure gradient to drive the mass flow of carbohydrates, is currently the most accepted model for such sucrose transport. When this hypothesis is combined with the conservation of fluid mass and momentum as well as sucrose mass, many simplifications must be invoked to mathematically close the problem and to resolve the flow. This study revisits such osmotically driven flows by developing a new two-dimensional numerical model in cylindrical coordinates for an elastic membrane and a concentration-dependent viscosity. It is demonstrated that the interaction between the hydrodynamic and externally supplied geometrical characteristic of the phloem has a significant effect on the front speed of sucrose transport. These results offer a novel perspective about the evolutionary adaptation of plant hydraulic traits to optimize phloem soluble compounds transport efficiency.

I. INTRODUCTION

The transport of soluble organic compounds within plants from production sites made during photosynthesis (i.e., leaves) to where sucrose consumption occurs (e.g., stems and roots) is receiving renewed attention in plant physiology, eco-hydrology, and earth systems models. The phloem provides the necessary pathway for this transport mechanism. Its structure and function have been conjectured to be optimized for efficient transport of photosynthates. The implications of efficient sucrose transport range from local impact on plant mortality under extreme weather conditions, such as drought,[1] to ecosystem-scale effects on carbon and water cycling because of the link between photosynthesis and sucrose transport.[2,3] Many models for phloem transport and their possible deficiencies have been formulated and discussed.[4–11] The most accepted hypothesis of which most of these models rely on is the so-called pressure-flow hypothesis, commonly known as the Münch mechanism.[4] In the pressure-flow hypothesis, the difference between the osmotic potential at the source and the sink leads to a pressure gradient along the phloem pathway necessary to drive the flow. The water reservoir needed for osmosis is provided by the xylem system, which is the other hydraulic network delivering water from roots to leaves under tension.[12]

Experimental challenges in measuring mass fluxes and pressure within the phloem[13,14] have led to reliance on theoretical approaches to predict sucrose transport. However, due to geometrical and hydrodynamic complexities of the phloem tissues, many simplifications have been used to allow mathematical tractability.[2,10,15] These simplifications have resulted in models that link the effects of a CO_2 enriched climate to plant growth[3,16] and the effect of environmental factors on plant hydraulic failure.[12,17–22] Nevertheless, such models remain silent on why measured leaf sugar concentrations are comparable to or even higher in shot crops than in tall trees.[23] Another critique is the presence of sieve plates throughout the phloem that appear to have no obvious advantage when viewed from the perspective of the Münch mechanism. Rather, the sieve plates seem to increase the flow resistance leading to increased pressure gradients to drive the flow that may not match the measured sugar concentrations in the leaves suggesting that phloem transport in tall trees is either a "miracle" or other mechanisms and adaptations are needed to compensate for the increased flow resistance.[17]

New theories have been formulated to add realism and improve the Münch mechanism. A recent study showed that the inclusion of the so-called Taylor dispersion can speed up the front speed.[10] In closed pipes, G.I. Taylor[24] showed that the small radial variations in solute concentration can have an impact on the front speed by adding an "extra" dispersion to the time evolution of solute mass. In osmotically driven flows through tubes made of semipermeable walls, the situation is different because of the radial inflow of water.[9] In such flows, there is another effect that arises from osmosis and can be modeled as an extra advection to the time evolution of solute mass. Another theory also showed that the inclusion of viscosity variations in the radial and axial direction due to local concentration variation can have an impact on the front speed independent of Taylor dispersion.[11] This latter study showed that the overall hydraulic conductivity of sieve elements is improved with a variable viscosity model especially in long-distance transport. Other theories have been also formulated by relying on the existence of sieve plates that connect the sieve tubes where their role is still not fully understood. One theory assumes that their role can be used as a "relay" effect where sugars can be exchanged at different locations along the phloem forming a relay system to increase efficiency and overcome the pressure gradient requirements brought by increased resistance.[25] While this theory is plausible, there is no clear evidence of loading and unloading sucrose along the phloem pathway, although water is exchanged between the phloem and surrounding tissues readily.[26–28] Another theory addresses the role of sieve plates from a structural damping perspective where their existence was conjectured to improve phloem rigidity and in return increases transport efficiency by reducing the radial expansion of the elastic conduits.[29]

The focus of this work is to explore these theories and conjectures using a two-dimensional numerical model. The model allows including membrane elasticity in a straightforward manner as well as a concentration dependent viscosity in contrast with previous models that span simplified one-dimensional cases with constant viscosity to two-dimensional cases that include variable viscosity but exclude elasticity.[30] This model enables the effect of membrane elasticity to be revealed beyond prior experiments studied elsewhere.[29] In addition, the model can be used to quantify the interactive effects of membrane elasticity and viscosity variations. The system of equations that describe the physics of sucrose transport in a semi-permeable elastic membrane is first presented in Sec. II. Next, the results that focus on the effect of membrane elasticity (prescribed via control parameters) and variable viscosity will be discussed in Sec. III. Finally, concluding remarks based on the modeling results are offered in Sec. IV regarding the evolutionary adaptation of plant hydraulic traits to maximize the phloem carbohydrate transport efficiency.

II. MODEL DEVELOPMENT

A. Problem setup

To develop the two-dimensional model for osmotically driven laminar flow within an elastic tube, certain assumptions are still required. The phloem is approximated as a long slender tube with length L and time-evolving radius $h(t)$ (i.e., $\varepsilon = h/L \ll 1$) where t is time and $t = 0$ being the initial loading of sucrose into the phloem. The initial radius commences at $h = a$ and expands radially in time (with no variability in the length). Since the radial inflow and outflow of water (due to osmosis as discussed later) is slow, the axial variations in the membrane radius h are assumed to be negligible. This assumption appears to be valid when images from published experiments on osmotically driven flows in an elastic tube have been analyzed.[29] The maximum radius that the membrane can attain is $2a$. The presence of sieve plates is not explicitly treated to remove any geometrical complexity. However, their impact on phloem transport can be included in two ways: reducing the elasticity of the membrane and increasing frictional losses. The focus here is on the first effect as the second effect appears to be small as discussed elsewhere[6] though there remains some disagreement on the significance of this loss.[17]

The sap is considered as an incompressible Newtonian fluid where the density $\rho = 1000$ kg m^{-3} does not depend on the sucrose concentration c. Theoretically, ρ depends on c; however, this variation is small and is assumed to be negligible for simplicity. On the other hand, the sap viscosity μ dependence on c is included since this dependence does impact the flow velocity.[11] For an order of magnitude illustration, increasing c from 10% wt/wt to 50% wt/wt increases ρ by a factor of 1.2, whereas μ increases by a factor of 4. The flow can be approximated as a low Reynolds number with $Re = \rho a u/\mu \ll 1$ where u is the longitudinal velocity component. For mass transport, the molecular Schmidt number Sc is defined here as Pe/Re, where $Pe = va/D$ is the radial Peclet number and v and D are the radial velocity component and molecular diffusion coefficient, respectively. It is assumed throughout that Sc is very large. These two properties of the flow imply that: (i) the inertial forces in the momentum balance can be neglected while keeping the advective transport terms in the solute mass balance and (ii) the momentum balance can be assumed to be steady, while the solute mass balance is transient.

Dealing with a moving domain (expanding tube) adds complexity to the numerical scheme that is accommodated using a coordinate transformation. The equations are expressed in cylindrical coordinates where only x, being the longitudinal direction, and r, being the radial direction, are considered because of cylindrical symmetry. Since radially r goes from zero (at the center of the tube) to $h(t)$ (membrane's radius), the domain is radially increasing in time. In this case, to transform the domain into a fixed one, the following change of variable is used: $y = r/h$, where y now goes from zero to unity. Since the h only depends on time t and not x, the derivatives in the new coordinate system are related to the original coordinate system through the chain rule,

$$\frac{\partial}{\partial r} = \frac{1}{h}\frac{\partial}{\partial y}, \quad \frac{\partial}{\partial x} = \frac{\partial}{\partial x}, \quad \frac{\partial}{\partial t} = \frac{\partial}{\partial t} - \frac{y}{h}\frac{dh}{dt}\frac{\partial}{\partial y}. \tag{1}$$

These relations can now be used to develop the required equations for the numerical model. Figure 1 shows a schematic representation of the flow and the coordinate systems. Since the nondimensional form of the equations will be used, the normalized variables are defined as follows: $x = LX$, $r = aR$, $h = aH$, and $y = H$ (where the last scaling arises from its definition). The use of nondimensional form is necessary to simplify the problem into its leading order result as discussed later.

B. Hydrodynamics

Three conservation laws are needed to develop the hydrodynamics model: (i) conservation of fluid mass (i.e., continuity equation),

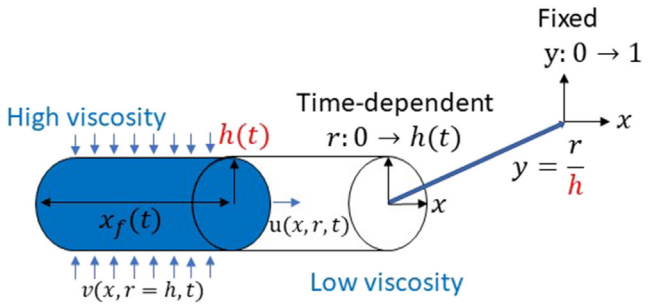

FIG. 1. A schematic representation of osmotically driven laminar flows within an elastic membrane. The terms u, v, x_f, and h are the axial and radial velocities, front position, and membrane radius, respectively. The x and r are the longitudinal and radial directions, and y is the radial direction in the new coordinate system with a fixed domain.

(ii) conservation of momentum in the axial and radial directions only due to cylindrical symmetry, and (iii) conservation of solute mass (i.e., advection–diffusion equation). As mentioned earlier, these equations will be expressed in a nondimensional form to enable further simplifications for model development. The normalized variables defined by $u = u_0 U$, $v = v_0 V$, $\mu = \mu_0 \hat{\mu}$, $p = p_0 P$, $c = c_0 C$, and $t = t_0 \tau$ are introduced, where u_0, v_0, μ_0, p_0, c_0, and t_0 are the characteristic axial velocity, radial velocity, dynamic viscosity, pressure, concentration, and time, respectively.

The characteristic concentration c_0 is set to be in grams, and μ_0 is determined from c_0 (converted into mol m^{-3}) and temperature T following a typical relation between concentration and dynamic viscosity for sucrose.[31] The characteristic radial velocity v_0 is determined from osmosis (the driving force for this type of flow) as later discussed, and u_0 is related to v_0 by the aspect ratio ε as $u_0 = v_0/\varepsilon$. The characteristic pressure is set by the viscous pressure scale as $p_0 = L\mu_0 u_0 a^{-2}$ (since the flow is at low Reynolds and Münch numbers[10]) and the characteristic time is the radial diffusion timescale, which is the fastest physical process in this case, as $t_0 = a^2/D$.

For an incompressible Newtonian fluid, the nondimensional form of the continuity equation in the new coordinate system (i.e., $x - y$ system) is

$$H\frac{\partial U}{\partial X} + \frac{1}{Y}\frac{\partial}{\partial Y}(YV) = 0, \tag{2}$$

where H, U, and V are the membrane radius and axial and radial velocity in a nondimensional form, respectively. Equation (2) is true when the viscosity is allowed to vary with solute concentration or when it is assumed to be constant, set by the loading concentration. Both cases will be analyzed to allow the effect of membrane elasticity alone (by assuming a constant viscosity) and the interactive effects of both to be evaluated. However, only the momentum conservation equations of the constant viscosity case will be shown for simplicity. The full Navier–Stokes equations for the variable viscosity case can be derived and is featured elsewhere.[11] Here, only the leading order results are shown.

The flow of water in the tube is described by the momentum balance in the axial and radial directions, which are shown here in a nondimensional form as

$$\begin{aligned}
&\frac{\varepsilon}{Sc}\left[\frac{\partial U}{\partial \tau} - \frac{Y}{H}\frac{dH}{d\tau}\frac{\partial U}{\partial Y}\right] + \varepsilon Re\left[U\frac{\partial U}{\partial X} + \frac{V}{H}\frac{\partial U}{\partial Y}\right] \\
&\quad = -\frac{\partial P}{\partial X} + \varepsilon^2\frac{\partial^2 U}{\partial X^2} + \frac{1}{YH^2}\frac{\partial}{\partial Y}\left(Y\frac{\partial U}{\partial Y}\right) \\
&\frac{\varepsilon^3}{Sc}\left[\frac{\partial V}{\partial \tau} - \frac{Y}{H}\frac{dH}{d\tau}\frac{\partial V}{\partial Y}\right] + \varepsilon^3 Re\left[U\frac{\partial V}{\partial X} + \frac{V}{H}\frac{\partial V}{\partial Y}\right] \\
&\quad = -\frac{1}{H}\frac{\partial P}{\partial Y} + \varepsilon^4\frac{\partial^2 V}{\partial X^2} + \varepsilon^2\frac{1}{YH^2}\frac{\partial}{\partial Y}\left(Y\frac{\partial V}{\partial Y}\right) - \varepsilon^2\frac{V}{Y^2H^2},
\end{aligned} \tag{3}$$

where $Re = \rho u_0 a \mu_0^{-1}$ and $Sc = Pe/Re$ are the Reynolds and Schmidt numbers, respectively, as before. Equation (3) assumes that there are no external forces on the fluid and that gravitational forces are negligible.[6] As in the lubrication theory, when the reduced Reynolds number tends to zero (i.e., $\varepsilon Re \to 0$) and for high Schmidt number (i.e., $Sc \gg 1$), the leading order terms in Eq. (3) satisfy

$$\frac{1}{YH^2}\frac{\partial}{\partial Y}\left(Y\frac{\partial U}{\partial Y}\right) = \frac{\partial P}{\partial X}, \quad \frac{1}{H}\frac{\partial P}{\partial Y} = 0. \tag{4}$$

The boundary conditions needed to obtain the leading order terms of the velocity field from Eq. (4) are as follows:

$$U(Y = 1) = 0, \quad \left.\frac{\partial U}{\partial Y}\right|_{Y=0} = 0, \quad V(Y = 0) = 0. \tag{5}$$

The first boundary condition in Eq. (5) states a no-slip condition at the membrane. The second and third boundary conditions are derived from symmetry considerations alone at the center of the pipe. Combining Eqs. (4) and (2), the axial and radial velocities are given by

$$U = \frac{H^2}{4}\frac{\partial P}{\partial X}[Y^2 - 1], \quad V = -\frac{H^3}{8}\frac{\partial^2 P}{\partial X^2}\left[\frac{Y^3}{2} - Y\right]. \tag{6}$$

From Eq. (6), one can see that the formulation is the same as the Hagen–Poiseuille formulation with two differences: (i) The pressure gradient $\partial P/\partial X$ is not constant because osmosis dictates a finite radial velocity at the membrane leading to $\partial^2 P/\partial X^2 \neq 0$ and (ii) the membrane radius is not constant and appears as a new variable H to be calculated from a separate equation discussed later on that accommodates wall elasticity and permeability. The velocity field for a variable viscosity can be derived in a similar manner where the full details are shown in Ref. 11 with the derivation in the new coordinate systems not differing from the case of constant viscosity. The velocity field can be determined from

$$\begin{aligned}
\hat{\mu}\frac{\partial U}{\partial Y} &= \frac{Y}{2}H^2\frac{\partial P}{\partial X} \\
H\frac{\partial U}{\partial X} + \frac{1}{Y}\frac{\partial}{\partial Y}(YV) &= 0.
\end{aligned} \tag{7}$$

The first equation of (7) results from the axial momentum balance equation that differs from Eq. (4) by having a concentration-dependent viscosity multiplying the term on the left-hand side and a new term that includes the first derivative of the viscosity $\partial\hat{\mu}/\partial Y$ multiplied by the first derivative of the axial velocity $\partial U/\partial Y$ as shown in Ref. 11. After re-arranging these terms together in a similar manner as in Eq. (4) (where $\hat{\mu}$ appears inside the derivative), one can integrate this equation in the Y direction to arrive at the result in Eq. (7) while imposing the second boundary condition of Eq. (5). Inspecting

Eq. (7), it is noted that when the viscosity is constant, the result in Eq. (6) can be derived from Eq. (7) as expected.

The third conservation law, the conservation of solute mass, is derived using the Reynolds transport theorem. The transport of solutes (here sucrose) in the axial and radial directions follows from advection and molecular diffusion. The equation for the conservation of solute mass in a nondimensional form can be expressed as (in the $X-Y$ coordinate system)

$$\frac{\partial C}{\partial \tau}-\frac{Y}{H}\frac{dH}{d\tau}\frac{\partial C}{\partial Y}+Pe\,U\frac{\partial C}{\partial X}+Pe\frac{V}{H}\frac{\partial C}{\partial Y}=\varepsilon^2\frac{\partial^2 C}{\partial X^2}+\frac{1}{YH^2}\frac{\partial}{\partial Y}\left(Y\frac{\partial C}{\partial Y}\right), \tag{8}$$

where $Pe=v_0h_0D^{-1}$ is the radial Peclet number as discussed earlier. Equation (8) describes the conservation of solute mass for the constant and variable viscosity cases. The new term on the left-hand side is the result of a radially expanding membrane where the nondimensional membrane radius H is a function of dimensionless time τ.

As discussed earlier, osmotically driven flows differ from the Hagen–Poiseuille formulation because of the radial inflow and outflow of water. In this case, the membrane is semi-permeable and allows water molecules to enter and exit the tube, but it conserves the solute molecules within the tube. The radial inflow/outflow of water along the tube boundaries arises from a pressure difference across the membrane due to osmosis. It is best formulated as a boundary condition (in a nondimensional form) using a Darcy-type flow expression[32] as

$$V=MP-\frac{C}{H^2}+\alpha_1\frac{1}{Pe}\frac{dH}{d\tau}, \tag{9}$$

where $M=k\mu_0L^2a^{-3}$ is the Münch number defined as the ratio of axial to radial resistance,[7,10] and α_1 is a constant related to membrane properties. The membrane permeability k is assumed constant in space and time (i.e., no permeability variations due to membrane expansion) for simplicity. Theoretically, k is not constant (especially in time), where the membrane's pores distribution and size are varying because of the membrane expansion. This assumption is especially invalid if the membrane is allowed to reach its plastic regime where the material is deformed. However, to reduce the number of model parameters that must be *a priori* specified, the membrane is assumed to be ideally elastic with a constant k. Equation (9) is evaluated at $Y=1$ and describes the driving force in this type of flow where the radial velocity scale $v_0=kR_gTc_0(M_w\pi L)^{-1}h_0^{-2}$ is obtained [$R_g=8.3145\,\mathrm{J\ (mol\ K)^{-1}}$, $T=293\,\mathrm{K}$, and $M_w=342.3\,\mathrm{g\ mol^{-1}}$ are the ideal gas constant, temperature, and sucrose molecular weight, respectively]. The last term on the right-hand side of Eq. (9) arises due to changing the coordinate system. This term describes the work done against the membrane to expand it.[29] In this case, V becomes the relative velocity in the moving frame of reference and $V-\alpha_1 dH/d\tau$ describes the absolute velocity needed for osmosis. The choice for the constant α_1 and its effect on the flow will be discussed in Sec. III.

C. Membrane elasticity

To understand the time evolution of the membrane radius, specification of the membrane physics is necessary. This specification can be accomplished by considering the fluid–solid interface interactions and analyzing the stresses and deformation within the membrane. However, since the main concern here is to analyze the effect of membrane elasticity on osmotically driven flow numerically, a simpler approach will be adopted. From independent experiments on elastic permeable tubes,[29] the membrane radius appears to evolve in a near exponential manner with increasing t. For this reason, a differential equation that leads to an exponential shape will be externally supplied so that

$$\frac{dh}{dt}+a_1h=a_2, \tag{10}$$

where a_1 and a_2 are two constants that both depend on membrane properties (rigidity and elastic properties). The nondimensional form of Eq. (10) can now be written as

$$\frac{dH}{d\tau}+E_1H=E_2, \tag{11}$$

where $E_1=a_1t_0=1/r_a$ and $E_2=a_2t_0/h_0=m/r_a$ are two nondimensional numbers related to the rate of expansion factor r_a (i.e., if $r_a=2$, the rate of expansion is $2t_0$) and the maximum radius factor m (i.e., if $m=2$, the maximum radius is $2a$). These two constants describe two separate features of the membrane, which we label as elasticity and rigidity. Here, elasticity describes the temporal rate of membrane expansion (higher rate of expansion means lower elasticity), whereas rigidity refers to the maximum radius that can be achieved by the membrane tube before plastic behavior dominates. That is, a higher maximum radius factor means a lower rigidity. It is noted that imposing such a representation on h or H weakens the coupling between fluid pressure and expansion rates. This coupling may be added by allowing a_1 to be transient and vary with fluid pressure in the tube. For simplicity, this addition was not included and only the magnitude of a constant a_1 is considered. To be clear, a_1 dictates the rate of tube expansion, but the final tube radius (maximum volume) that can be attained is set by a_2. Including a dependency between a_1 and fluid pressure will act to alter the time at which the maximum expansion is reached, but not its magnitude.

D. Model calculation

1. Numerical scheme

A brief description of the numerical scheme is presented. In plants, the radial Peclet number Pe is small thus characterizing a predominately diffuse flow and for the results presented in Secs. III A–III C, the Pe was chosen to be less than unity. For this reason, a central difference approximation was used to develop the numerical scheme with 50 nodes in both directions (axial and radial). For the time marching scheme, an iterative approach was used to calculate the concentration and membrane radius from Eqs. (8) and (11). At each time step, the velocity and pressure fields are solved by discretizing the equations while using the previous concentration field and membrane radius. For the constant viscosity model, Eq. (9) is used to solve the pressure field in the domain while noting that $V|_{Y=1}$ can be related to P from the second equation of (6) and $dH/d\tau$ can be obtained from Eq. (11). For the variable viscosity model, Eqs. (7) and (9) are used. Then, the concentration field and membrane radius are solved using Eqs. (8) and (11) using the explicit scheme. Within each time step, the following recurrence scheme is used $F_{k+1}=\beta F_{k+1}+(1-\beta)F_k$. That is, from F_k, an F_{k+1} is determined and a weighing scheme between

these two values is employed to re-determine F_{k+1}. F_{k+1} on the right-hand side is an estimate to be adjusted based on the weight β. This recurrence scheme has been used to accommodate the non-linearity of including a concentration-dependent viscosity. (For consistency, it is also used for the constant viscosity model.) In this case, at each iteration, the viscosity is solved using the concentration at iteration $k+1$ and the velocity and pressure fields are solved the same as before. Once convergence is achieved (i.e., the root mean square error between $k+1$ and k for C and H), the numerical model goes into the new time step. The β is a constant ranging from zero to unity describing the weight taken from each new iteration. For example, if $\beta = 0$, the scheme becomes the common explicit scheme in time with no iteration within each time step. If $\beta = 1$, the scheme behaves like an implicit scheme in time. For the set of conditions chosen and presented later, $\beta = 0.1$ and the non-dimensional time increment was set to $d\tau = 0.001$. The scheme was tested using multiple values of β, and the solution was shown to be independent $d\tau$ or *beta* in the vicinity of those selected values. For boundary conditions, closed pipe boundary conditions (i.e., $U(X=0) = U(X=1) = 0$) were chosen for the longitudinal velocity fields beside the ones in Eqs. (5) and (9). Additionally, the closed tube assumption with no sinks requires the solute to be conserved within the tube so that

$$\left.\frac{\partial C}{\partial X}\right|_{X=0} = \left.\frac{\partial C}{\partial X}\right|_{X=1} = 0,$$
$$Pe\, H(VC)|_{Y=1} - \left.\frac{\partial C}{\partial Y}\right|_{Y=1} = 0. \tag{12}$$

Symmetry considerations at the center of the tube $\partial C/\partial Y|_{Y=0}$ were enforced here. For initial conditions, sucrose was released as an axially smooth function (i.e., $C(X, \tau = 0) = f(X)$) with no radial variation and the membrane radius was set to unity (i.e., starting at the initial radius a).

2. Front position

The front position x_f can be used to assess the transport efficiency for different cases. This front position can be calculated numerically from maximal $|\partial\overline{C(X)}/\partial X|$ where the overline operator denotes area-averaging in the radial direction. Based on previous studies,[7,29] the evolution of the front position follows an approximate exponential profile given by

$$x_f = L - (L - l)\exp(-\theta t), \tag{13}$$

where $l = 0.2$ is the initial sucrose front location, $L = 1$ is the length of the tube, and x_f is the front position all in non-dimensional form. From Eq. (13), one can obtain a linear relation between t and $ln[(L - x_f)/(L - l)]$. Hence, linear regression can be used to calculate the constant θ describing the rate of evolution of the front position away from the entrance boundary condition. For reference, this evaluation was conducted when the front reaches around 50% of the domain (i.e., maximum distance away from the imposed boundaries longitudinally).

III. RESULTS AND DISCUSSION

The results presented here highlight the effect of having an idealized elastic membrane (i.e., uniformly expanding in the radial direction) instead of a rigid one on osmotically driven laminar flows for both constant and variable viscosity models. The analysis can be divided into three parts. In the first part, the analysis will focus on varying the rate of expansion factor r_a that describes the elasticity of the membrane. In the second part, the analysis will focus on varying the maximum radius factor m that describes the rigidity of the membrane. Finally, the analysis will focus on the interconnected effect between having a concentration dependent viscosity and the membrane elasticity and rigidity.

Typical phloem conditions were used to generate the results for comparison: initial membrane radius $a = 10\,\mu$m, tube length $L = 0.1$ m, membrane permeability $k = 10^{-12}$ m (Pa s)$^{-1}$, molecular diffusion of sucrose in water $D = 4 \times 10^{-10}$ m^2 s^{-1}, loading sucrose concentration $c_0 = 10^{-5}$ g, and dynamic viscosity μ_0 calculated from c_0 and T based on a neural network model.[31] For these conditions, the nondimensional numbers are $Re = 0.0632$, $\varepsilon Re = 6.3183 \times 10^{-6}$, $M = 0.0359$, $Pe = 0.0566$, and $Sc = 8.9637 \times 10^3$. Clearly, the order of magnitude of these nondimensional numbers will have an impact on the flow as shown in previous studies.[7,10,11] However, since the main concern here is the effect of membrane elasticity and its relation with variable viscosity, only the results of this set of conditions are shown.

For membrane properties, there is substantial uncertainty (i.e., order of magnitude is not known) on the rigidity of the membrane. Another complication to describing membrane rigidity in real trees is that rigidity will also depend on the turgor of the surrounding cells.[33] For this reason, the constants r_a, m, and α_1 were chosen as constants and sensitivity analyses around those values conducted. For the rate of expansion, two cases were chosen: $r_a = 5$ and $r_a = 10$. For the maximum radius factor, also two cases were chosen: $m = 1.5$ and $m = 2$. For α_1, the values were chosen depending on the average pressure in the membrane. Based on previous experiments,[29] the axially averaged pressure follows the profile of the radius evolution in time. By averaging Eq. (9) in the longitudinal direction, one can see that the average pressure is close to the average osmotic potential minus the rate of expansion of the membrane. This finding is theoretically consistent with the findings in Ref. 29 (since $\int V dX = 0$ because of the closed boundary conditions at both end of the membrane). For $r_a = 5$ and $r_a = 10$, $\alpha_1 = 1$ and $\alpha_1 = 2$ were chosen, respectively, that lead to necessary exponential profile of the average pressure evolution in time as shown in Fig. 2(a). The choice of α_1 did not have any primary impact on the front speed, where the case of $r_a = 10$ and $\alpha_1 = 1$ was assessed for the constant and variable viscosity models (not shown). However, it did have an impact on the average pressure profile where there was an initial drop in the pressure (again not shown) because it followed the average osmotic potential, which is decreasing as shown in Eq. (9) (because H is increasing). Theoretically, α_1 should not have an impact on the front speed because the axial velocity depends on the pressure gradient and not on the absolute pressure. If one differentiates Eq. (9), the rate of expansion of the membrane radius term disappears because of the assumption $H \neq f(X)$ as discussed in Sec. II A. Finally, the rigid case was chosen when $E_1 = 0$ and $E_2 = 0$ leading to five cases in total for each model.

A. Effect of membrane's rate of expansion

As discussed in Sec. II C, the rate of expansion parameter r_a is related to the membrane elasticity. When r_a decreases, the elasticity of

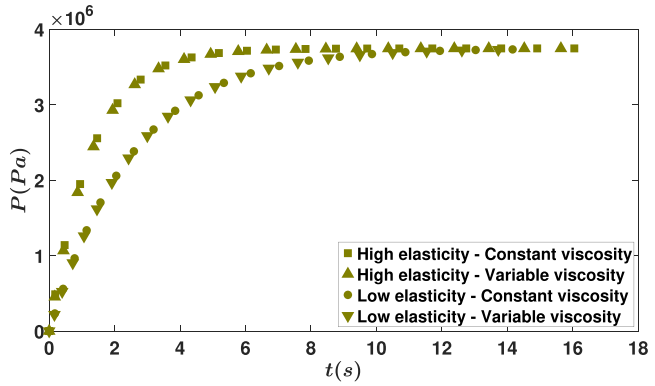

(a)

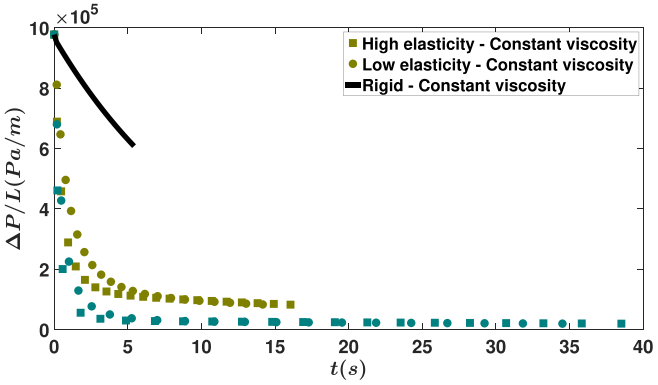

(b)

FIG. 2. (a) The time evolution of average pressure in the tube and (b) the time evolution of the pressure gradient along the domain. Square and up-pointing triangle denote the constant and the variable viscosity model with high elasticity ($r_a = 5$), respectively. Circle and down-pointing triangle denotes the constant and the variable viscosity models with low elasticity ($r_a = 10$), respectively. Solid black line denotes the constant viscosity model for a rigid membrane. Different colors denote different maximum radius (i.e., different m).

the membrane increases and the membrane reaches its maximum expanded radius faster. This result can be first shown when one considers the pressure gradient over the domain which is shown in Fig. 2(b). For both cases of m, when the membrane elasticity is lower, the pressure gradient is higher compared to the higher elasticity case. Having a higher pressure gradient leads to a higher axial velocity as predicted from Eq. (6). Here, only the constant viscosity model is shown since the variable viscosity model has a similar behavior but with a lower magnitude[11] (i.e., higher efficiency). The effect of membrane elasticity can also be shown in Fig. 3 that shows the evolution of the membrane radius in time. This has an impact on the evolution of sucrose front, where simulation results show that the front travels faster when the membrane is less elastic. This result is apparent in Fig. 4(a) that features the evolution of the front position in time. From this figure, one can see that the front reaches the mid-point of the domain faster when the membrane has lower elasticity (i.e., higher r_a) for both models. This effect is independent of the maximum radius that the membrane can reach (i.e., for both cases where $m = 1.5$ and $m = 2$),

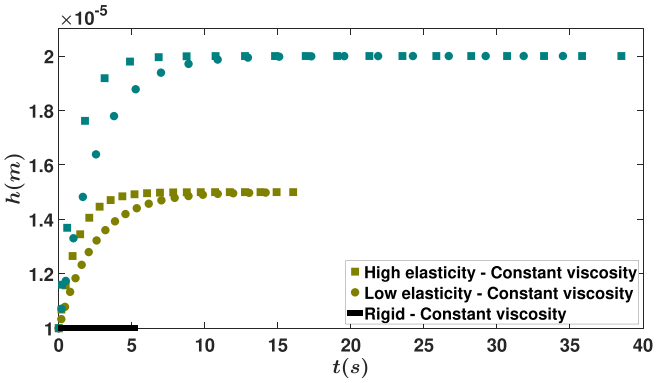

FIG. 3. The time evolution of membrane radius. Square denotes the constant viscosity model with high elasticity $r_a = 5$. Circle denotes the constant viscosity model with low elasticity $r_a = 10$. Solid black line denotes the constant viscosity model for a rigid membrane. Blue color denotes the case $m = 2$, and green color denotes the case $m = 1.5$.

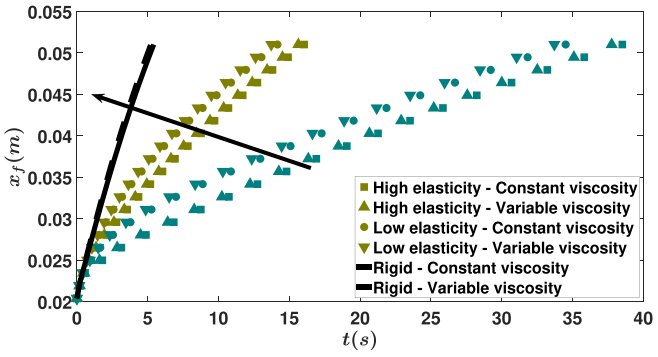

(a)

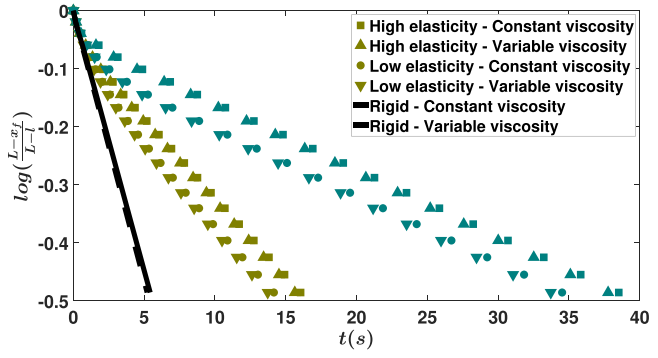

(b)

FIG. 4. (a) The time evolution of the front position x_f and (b) the time evolution of the logarithm of the relative front position. Square and up-pointing triangle denote the constant and the variable viscosity model with high elasticity ($r_a = 5$), respectively. Circle and down-pointing triangle denote the constant and the variable viscosity models with low elasticity ($r_a = 10$), respectively. Solid black line denotes the constant viscosity model for a rigid membrane. Dashed black line denotes the variable viscosity model for a rigid membrane. Different colors denote different maximum radii (i.e., different m). Head of the arrow in (a) shows the direction of increased rigidity.

which is more apparent in Fig. 4(b) that shows the logarithm of the relative front position as a function of time as discussed in Sec. II D 2. Again, Fig. 4(b) shows that for each case (both m and both models), θ decreases with elasticity. Since the rigid case for each models has the highest transport efficiency, the ratio θ/θ_r, where θ_r is the θ for the rigid case, shows the degree of efficiency. Taking the constant viscosity model, for example, for $m = 1.5$, the ratio is equal to 0.3237 when r_a and 0.3685 when $r_a = 10$ and for $m = 2$, the ratio is equal to 0.1337 ($r_a = 5$) and 0.146 ($r_a = 10$). As expected, this means that for lower elasticity, the transport efficiency is higher. The variable viscosity model had a similar pattern.

B. Effect of membrane's maximum radius

Having covered the effects of elasticity on front speed for two prescribed rigidity values, we now turn attention to the rigidity effects on front speed for two prescribed elasticity values. Recall that the rigidity effects are reflected by the parameter m as discussed in Sec. II C. When m increases, the maximum radius that the membrane can reach increases as shown in Fig. 3 (as expected from the definition of m). Simulation results show that increasing m (i.e., decreasing the membrane rigidity) leads to a slower front speed. Figure 2(b) shows this result where for the same r_a, the pressure gradient decreases with increasing m. This is also shown in Fig. 4(a) where the direction of the arrow shows the direction of increased rigidity. As expected, the sucrose front moves faster in a rigid membrane and this speed decreases whenever the membrane is allowed to expand. Again, the result is more visible using Eq. (13) to solve for θ for each case and is plotted in Fig. 4(b) where θ is the slope of each plot. As discussed in Sec. III A, the ratio θ/θ_r shows the degree of efficiency for each model when compared to the rigid (most efficient) case. For the constant viscosity model, when $r_a = 5$, this ratio is equal to 0.3237 when $m = 1.5$ and 0.13 when $m = 0.13$. When $r_a = 10$, this ratio is 0.36 when $m = 1.5$ and 0.15 when $m = 2$. Again, a similar behavior was apparent for the variable viscosity model. This finding underscores the role of membrane rigidity: For higher rigidity, sucrose transport efficiency is higher, as expected. These results are further elaborated upon when Eq. (9) is the driving force for this type of flow. When m increases, the maximum H increases leading to a lower osmotic potential (second term on the right in the equation) that drives the flow. In this case, the same amount of sugar is attained but in a higher volume of water. Increasing the volume of water without altering the sugar mass leads to a lower concentration and concomitant osmotic potential. This volume increase is in contrast to the rigid case where the osmotic potential is constant because the same water volume is sustained during the whole simulation. This contrast between the flexible and rigid membrane leads to the so-called dilution effect already discussed in laboratory studies.[29]

C. Impact of variable viscosity in an elastic membrane

As discussed in Secs. III A and III B, the variable viscosity model showed a similar trend in time as the constant viscosity model for all combinations of m and r_a with a minor difference. This difference is, once again, connected to the front speed. From Figs. 4(a) and 4(b), the sucrose front travels faster in the variable viscosity model when compared to the constant viscosity model for all m and r_a values. This front speed difference is not expected to be large given the small initial concentration c_0 and tube length L used here. In a recent study, it was shown that this difference in the front speed increases with increasing c_0 and increasing tube length due to viscosity variations.[11] However, the main concern here is the interactive effect between a concentration dependent viscosity and an elastic membrane and their concomitant trends on x_f. To study this effect, the initial concentration was doubled (i.e., $c_0 = 2 \times 10^{-5}$ g) and the efficiency coefficient $\theta/\theta_0 = \zeta$, where in this case β_0 is the calculated β (approximated from linear regression) for the constant viscosity model for each case (i.e., different m and r_a), is calculated. In this case, the increase in efficiency due to a concentration dependent viscosity compared to a constant one set by c_0 is calculated and compared when the rigidity (i.e., m) and elasticity (i.e., r_a) are changed. The results of this case are shown in Fig. 5(a) and demonstrates a similar trend as in Fig. 4(b). Using this analysis, the sensitivity of the variable viscosity model to both membrane parameters m and r_a can be further elaborated. For $r_a = 5$, $\zeta \sim 1.6$ when $m = 1.5$ and $\zeta \sim 1.3$ when $m = 2$. For $r_a = 10$, $\zeta \sim 1.9$ when $m = 1.5$ and $\zeta \sim 1.5$ when $m = 2$. From these results, one can see that the impact of a concentration dependent viscosity decreases when

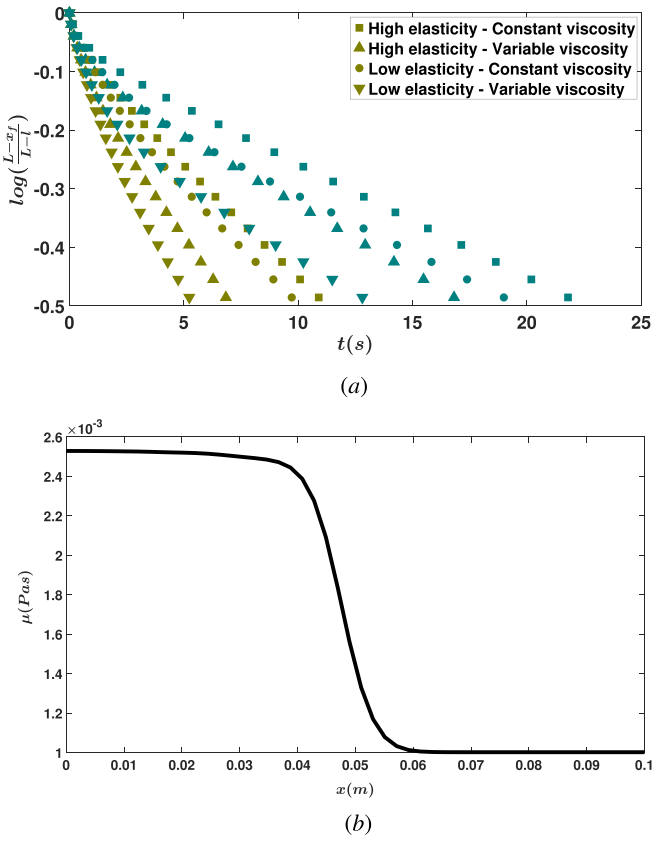

FIG. 5. (a) The time evolution of the logarithm of the relative front position for the higher concentration case $c_0 = 2 \times 10^{-5}$ g and (b) the viscosity profile along the longitudinal direction when the front reaches 50% of the domain. Square and up-pointing triangle denote the constant and the variable viscosity model with high elasticity ($r_a = 5$), respectively. Circle and down-pointing triangle denote the constant and the variable viscosity models with low elasticity ($r_a = 10$), respectively. Different colors denote different maximum radii (i.e., different m).

the membrane elasticity increases (i.e., decreasing r_a) and increases when the membrane rigidity increases (i.e., decreasing m). This result is related to the effect of local viscosity variations on the front speed, which is associated with a push-pull mechanism in osmotically driven flow as discussed in Ref. 11. Figure 5(b) shows the viscosity profile for the radially averaged concentration along the longitudinal direction (x) when the front reaches 50% of the domain. This profile is the same for all cases since the concentration does not differ from one case to another in a fixed domain. One can see from this figure that the efficiency of the flow can increase even if the viscosity only increases by a factor of 2. In summary, when changes in local viscosity are taken into consideration, the pull of water from the membrane (or the phloem in this case) to the surrounding water reservoir (or the xylem in this case) becomes more efficient because of decreased resistance to the flow. In this case, if the membrane is allowed to expand, more water molecules are being stored inside the membrane (hence the increase in volume) and that in return decreases the efficiency of the pull mechanism.

IV. CONCLUSIONS

The derivation of a two-dimensional numerical model for osmotically driven laminar flows within an elastic membrane was presented and discussed. This model also included local variations of viscosity due to sucrose concentration variations. The complexity of membrane elasticity was reduced to an imposed equation for the evolution of the membrane radius due to the lack of information on membrane elastic properties. In this case, the interplay between pressure variations and membrane elasticity, which does not affect front speeds since the driving force of the flow depends on the pressure gradient and not the absolute pressure, was not included. Nevertheless, this model captures the required representation of a fluid flow within an elastic membrane, which lead to certain implications on osmotically driven laminar flows. These implications were observed on the front speed, which is the target variable when studying the transport efficiency especially for this application (i.e., sucrose transport in the phloem). In summary, when the membrane is allowed to expand, thus acting as a water reservoir, the efficiency of the osmotic potential leads to a front that travels at a slower rate. This reduction in the flow rate is due to the fact that a part of the osmotic potential was lost because of dilution where more water was added to the membrane (capacitive effect) while keeping the same number of sugar molecules. This effect can be directly seen and assessed in the osmotic equation. The second effect is that a part of the osmotic potential was lost to expand the membrane. This effect cannot be explicitly seen in this model. Therefore, a more comprehensive approach that includes energy conservation and forces on the membrane interface is needed. The local variations in viscosity also act to increase the transport efficiency. The interesting impact of membrane elasticity was the decrease in transport efficiency due to local viscosity variations. These results have specific implication on sucrose transport within the phloem where they support the theory that the role of sieve plates is structural leading to hydraulic benefits. In this case, in plants, sieve plates are adding rigidity to the phloem for two reasons: (i) decrease the loss of energy due to membrane expansion and (ii) improve the flow enhancing effect of local viscosity variations. Future development will be on explicitly representing the sieve plates within the phloem and study their effect on adding frictional losses to the flow and improve the membrane equation to further estimate the loss of osmotic potential due to the work done on the membrane.

ACKNOWLEDGMENTS

This work was supported by the U.S. National Science Foundation (Nos. NSF-IOS-1754893 and NSF-AGS-2028633), the U.S. Department of Energy (No. DE-SC0022072 and DE-SC0023309), and the Los Alamos Directed Research and Development Exploratory Research Grant (No. 2020109DR).

AUTHOR DECLARATIONS

Conflict of Interest

The authors have no conflicts to disclose.

Author Contributions

Mazen Nakad: Conceptualization (lead); Formal analysis (lead); Investigation (lead); Methodology (lead); Writing – original draft (lead); Writing – review & editing (lead). **Jean-Christophe Domec:** Funding acquisition (equal); Formal analysis (supporting); Investigation (supporting); Methodology (supporting); Writing – review & editing (equal). **Sanna Sevanto:** Formal analysis (supporting); Investigation (supporting); Methodology (supporting); Writing – review & editing (equal). **Gabriel Katul:** Conceptualization (equal); Formal analysis (equal); Investigation (equal); Methodology (equal); Funding acquisition (equal); Writing – review & editing (equal).

DATA AVAILABILITY

The data that support the findings of this study are available from the corresponding author upon reasonable request.

REFERENCES

[1]S. Sevanto, N. G. Mcdowell, L. T. Dickman, R. Pangle, and W. T. Pockman, "How do trees die? a test of the hydraulic failure and carbon starvation hypotheses," Plant, Cell Environ. **37**, 153–161 (2014).
[2]E. Nikinmaa, T. Hölttä, P. Hari, P. Kolari, A. Mäkelä, S. Sevanto, and T. Vesala, "Assimilate transport in phloem sets conditions for leaf gas exchange," Plant, Cell Environ. **36**, 655–669 (2013).
[3]S. Fatichi, C. Pappas, J. Zscheischler, and S. Leuzinger, "Modelling carbon sources and sinks in terrestrial vegetation," New Phytol. **221**, 652–668 (2019).
[4]E. Münch, *Stoffbewegungen in Der Pflanze* (G. Fischer, Jena, Germany, 1930).
[5]R. Phillips and S. Dungan, "Asymptotic analysis of flow in sieve tubes with semi-permeable walls," J. Theor. Biol. **162**, 465–485 (1993).
[6]M. Thompson and N. Holbrook, "Application of a single-solute non-steady-state phloem model to the study of long-distance assimilate transport," J. Theor. Biol. **220**, 419–455 (2003).
[7]K. Jensen, E. Rio, R. Hansen, C. Clanet, and T. Bohr, "Osmotically driven pipe flows and their relation to sugar transport in plants," J. Fluid Mech. **636**, 371–396 (2009).
[8]P. Cabrita, M. Thorpe, and G. Huber, "Hydrodynamics of steady state phloem transport with radial leakage of solute," Front. Plant Sci. **4**, 531 (2013).
[9]S. Sevanto, "Phloem transport and drought," J. Exp. Botany **65**, 1751–1759 (2014).
[10]M. Nakad, T. Witelski, J. Domec, S. Sevanto, and G. Katul, "Taylor dispersion in osmotically driven laminar flows in phloem," J. Fluid Mech. **913**, A44 (2021).
[11]M. Nakad, J.-C. Domec, S. Sevanto, and G. Katul, "Radial-axial transport coordination enhances sugar translocation in the phloem vasculature of plants," Plant Physiol. **189**, 2061 (2022).
[12]W. Konrad, G. Katul, A. Roth-Nebelsick, and K. Jensen, "Xylem functioning, dysfunction and repair: A physical perspective and implications for phloem transport," Tree Physiol. **39**, 243–261 (2019).

[13]O. Curtis and H. Scofield, "A comparison of osmotic concentrations of supplying and receiving tissues and its bearing on the Münch hypothesis of the translocation mechanism," Am. J. Botany **20**, 502–512 (1933).
[14]T. Housley and D. Fisher, "Estimation of osmotic gradients in soybean sieve tubes by quantitative autoradiography: Qualified support for the Münch hypothesis," Plant Physiol. **59**, 701–706 (1977).
[15]K. Jensen, K. Berg-Sørensen, H. Bruus, N. Holbrook, J. Liesche, A. Schulz, M. A. Zwieniecki, and T. Bohr, "Sap flow and sugar transport in plants," Rev. Mod. Phys. **88**, 035007 (2016).
[16]M. Mencuccini and T. Hölttä, "The significance of phloem transport for the speed with which canopy photosynthesis and belowground respiration are linked," New Phytol. **185**, 189–203 (2010).
[17]J. Savage, S. Beecher, L. Clerx, J. Gersony, J. Knoblauch, J. Losada, K. Jensen, M. Knoblauch, and N. Holbrook, "Maintenance of carbohydrate transport in tall trees," Nat. Plants **3**, 965 (2017).
[18]C. Huang, J. Domec, S. Palmroth, W. Pockman, M. Litvak, and G. Katul, "Transport in a coordinated soil-root-xylem-phloem leaf system," Adv. Water Resources **119**, 1–16 (2018).
[19]S. Sevanto, "Drought impacts on phloem transport," Curr. Opin. Plant Biol. **43**, 76–81 (2018).
[20]Y. Salmon, L. Dietrich, S. Sevanto, T. Hölttä, M. Dannoura, and D. Epron, "Drought impacts on tree phloem: From cell-level responses to ecological significance," Tree Physiol. **39**, 173–191 (2019).
[21]C. Swanson and D. Geiger, "Time course of low temperature inhibition of sucrose translocation in sugar beets," Plant Physiol. **42**, 751–756 (1967).
[22]I. F. Wardlaw, "The control and pattern of movement of carbohydrates in plants," Botanical Rev. **34**, 79–105 (1968).
[23]M. Knoblauch, J. Knoblauch, D. Mullendore, J. Savage, B. Babst, S. Beecher, A. Dodgen, K. Jensen, and N. Holbrook, "Testing the Münch hypothesis of long distance phloem transport in plants," Elife **5**, e15341 (2016).
[24]G. Taylor, "Dispersion of soluble matter in solvent flowing slowly through a tube," Proc. Roy. Soc. London. Ser. A. Math. Phys. Sci. **219**, 186–203 (1953).
[25]A. Lang, "A relay mechanism for phloem translocation," Ann. Botany **44**, 141–145 (1979).
[26]M. Knoblauch and K. Oparka, "The structure of the phloem: Still more questions than answers," Plant J. **70**, 147–156 (2012).
[27]M. Knoblauch and W. Peters, "What actually is the Münch hypothesis? a short history of assimilate transport by mass flow," J. Integr. Plant Biol. **59**, 292–310 (2017).
[28]R. C. Stanfield, U. G. Hacke, and J. Laur, "Are phloem sieve tubes leaky conduits supported by numerous aquaporins?," Am. J. Botany **104**, 719–732 (2017).
[29]M. Nakad, J.-C. Domec, S. Sevanto, and G. Katul, "Toward a realistic representation of sucrose transport in the phloem of plants," J. Geophysical Res.: Biogeosciences **128**, e2022JG007361 (2023).
[30]T. Hölttä, M. Mencuccini, and E. Nikinmaa, "Linking phloem function to structure: Analysis with a coupled xylem–phloem transport model," J. Theor. Biol. **259**, 325–337 (2009).
[31]C. Bouchard and B. P. Granjean, "A neural network correlation for the variation of viscosity of sucrose aqueous solutions with temperature and concentration," LWT-Food Sci. Technol. **28**, 157–159 (1995).
[32]A. S. Iberall and A. M. Schindler, *Physics of Membrane Transport* (General Technical Services, 1973), Vol. 2.
[33]S. Sevanto, T. Hölttä, and N. M. Holbrook, "Effects of the hydraulic coupling between xylem and phloem on diurnal phloem diameter variation," Plant, Cell Environ. **34**, 690–703 (2011).